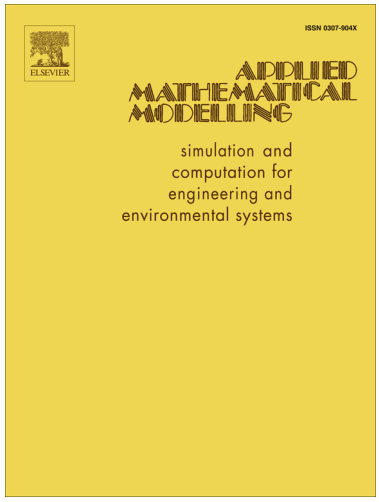


# Modelling, Analysis and Simulation of an Optical Squeezer

S.Z. Sayed Hassen

PII: S0307-904X(14)00666-0
DOI: http://dx.doi.org/10.1016/j.apm.2014.11.066
Reference: APM 10297

To appear in: *Appl. Math. Modelling*

Received Date: 11 December 2013
Revised Date: 12 November 2014
Accepted Date: 24 November 2014

Please cite this article as: S.Z. Sayed Hassen, Modelling, Analysis and Simulation of an Optical Squeezer, *Appl. Math. Modelling* (2014), doi: http://dx.doi.org/10.1016/j.apm.2014.11.066

# Modelling, Analysis and Simulation of an Optical Squeezer

S. Z. Sayed Hassen*

**Abstract**

Squeezed states of light have numerous potential applications ranging from gravitational wave detection, quantum teleportation, quantum cryptography and quantum communication. They are generated using an optical squeezer and possess the desirable property of having less noise in one quadrature than dictated by the quantum noise limit(QNL). In this paper, we model the nonlinear optical process by which squeezed light is generated in a classical framework and analyse its steady-state behaviour from a control theoretic perspective. In particular, through computer simulation, we provide a visual perspective of the effect of the steady-state operating point of the optical squeezer on the type of squeezed states of light generated.

*Keywords:* Nonlinear dynamics, Computational physics, Nonlinear oscillator, Frequency control, System Modeling and simulation

*Nomenclature*

| | |
|---|---|
| QNL | Quantum Noise Limit |
| SQL | Standard Quantum Limit |
| GWD | Gravitational Wave Detectors |
| EPR | Einstein-Podolsky-Rosen |
| OPA | Optical Parametric Amplifier |
| OPO | Optical Parametric Oscillator |
| SHG | Second Harmonic Generation |
| DFG | Difference Frequency Generation |

## 1. Introduction

It is well known in the physics literature that experiments performed at the quantum level are restricted by the quantum noise limit (QNL) [1]. The QNL sets a fundamental limit to the performance of quantum systems and puts a bound on the signal to noise ratio that can be achieved, restricting the usefulness of applications involving quantum technology. Advances in nano-technology and atomic systems have led to devices which are sensitive enough to detect quantities at a level where quantum effects become significant. Furthermore, with the use of nonlinear effects and nonlinear media in quantum optics [2, 3], it is possible to change the statistics of quantum noise, allowing for measurements that are better than permitted by the standard quantum limit (SQL). Here, SQL refers to the minimum level of quantum noise that can be obtained with the use of states of light that possess standard quantum noise properties.

If we define the amplitude and phase quadrature operators [4] of an optical field as $\mathbf{X}^{+}$ and $\mathbf{X}^{-}$ respectively, then the Heisenberg uncertainty principle [1, 5] implies that the variance of the operators in any given state is constrained by

$$\langle \Delta \mathbf{X}^{+^2} \rangle \langle \Delta \mathbf{X}^{-^2} \rangle \geq 1; \tag{1}$$

*Electrical & Electronic Engineering Dept.,University of Mauritius, Réduit, Mauritius Ph: + (230) 454 9215
*Email address:* sayed.hassen@gmail.com (S. Z. Sayed Hassen)

where $\langle\cdot\rangle$ denotes the quantum expectation value. In the case of laser light, which can be modeled as being in a coherent state $|\alpha\rangle$ [4] or minimum uncertainty state (with a minimal product of the amplitude and phase quadrature uncertainties), the uncertainty associated with the quantum state is equally divided between the two quadratures such that

$$\langle \Delta \mathbf{X}^{+^2} \rangle = \langle \Delta \mathbf{X}^{-^2} \rangle = 1. \tag{2}$$

The uncertainty can thus be visualised as shown in Figure 1, in what is known as the *ball on stick* diagram. The straight line is the coherent amplitude and the diameter of the ball (which has been blown up in scale in the picture) represents the variance of the respective quadratures. It is circular in this case indicating that noise in each quadrature is equal. The "uncertainty ball" arises as a result of the quantum nature of light, affecting a given system and restricts how close two measurable quantum states can be if they are to be distinguished from each other. Indeed, classical noises affect measurement of classical states in a similar fashion but they can however (in theory) be completely suppressed with improved measurement techniques. This is not the case for quantum noises whose sizes are dictated by the laws of quantum mechanics rather than as a result of the limitations of the measurement devices. It is possible, fortunately to partly circumvent this problem by concentrating the quantum noises in specific quadratures of light. In other words, we can rearrange the noise distribution between the quadratures such that one quadrature has less noise than the other. Quantum states of light which have this property of asymmetric quadrature noise distributions are known as "squeezed" or "non-classical" states of light.

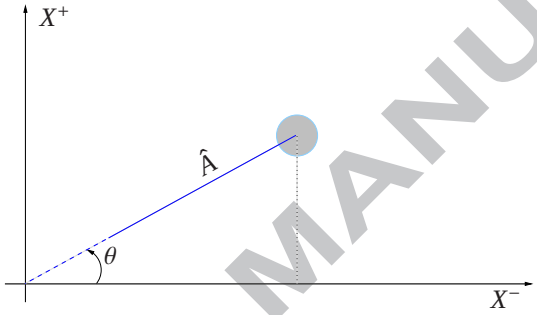


Figure 1: Minimum uncertainty state

## 2. Squeezed states

Some of the different types of squeezed states that can be achieved from a coherent state are shown in Figure 2. As mentioned before, squeezed states of light have their quantum noises squeezed and possess noise distribution which are less than those of the coherent states of light in *specified directions.*

A coherent state of light has a Gaussian distribution such that (2) is satisfied. Pauli [6] showed that both a coherent quantum state and squeezed state can be completely described using only 2-dimensional Gaussian distribution functions. For a squeezed state, the only requirement is that the width of these functions need to satisfy the uncertainty principle for any chosen direction $\theta$. The contour line for such a 2-dimensional function turns out to be always elliptical, while that for a coherent state is circular. The total area inside the contour can however never be less than that of the uncertainty area of a coherent state. For the case of phase squeezed states (Figure 2(b)), they have a narrow axis aligned with the phase axis and the widest distribution orthogonal to the phase axis. Similarly, for an amplitude squeezed state (Figure 2(c)), there is less noise along the amplitude quadrature and the fluctuations along the phase quadrature are above the standard quantum noise limit. In the presence of external sources of noise, both quadratures will be affected but as long as the excess noise introduced does not drive the fluctuations above the standard quantum noise limit, squeezed states are obtained. In this way, depending on whether the amplitude or the phase quadrature is being measured, the state can be squeezed accordingly such that the measurement can become more sensitive in a given direction. Moreover, a quantum state can be squeezed along any arbitrary angle with respect to the predefined amplitude and phase quadratures, as shown in Figure 2(d) and the state is then described as quadrature squeezed state.

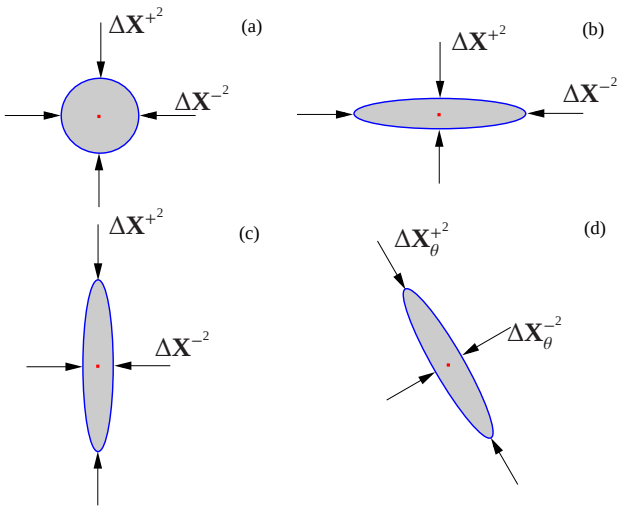


Figure 2: Quantum noises associated with different quantum states. (a) Coherent state, (b) Amplitude quadrature squeezed state, (c) Phase quadrature squeezed state, (d) Arbitrary (Quadrature) squeezed state.

Squeezed states are of course, going to be most useful in applications where the standard quantum noise limit has already been reached.

### *2.1. Applications of Squeezed states*

Squeezed states of light have a wide range of potential applications. One promising application of squeezed states of light is in gravitational wave detection [7, 8], where it can potentially improve the sensitivity of interferometers. Gravitational wave detectors (GWD) are currently optimized to operate at the quantum noise limit. The use of phase-squeezed light achieves a better signal to noise ratio than a standard GWD with the same laser power and may finally enable us to detect gravitational waves. Quantum teleportation, which is an integral part of quantum communication and information processing, has also been demonstrated using squeezed light [9]. Amplitude-squeezed light, on the other hand, is used for the measurement of weak spectroscopic signals. Other potential applications of squeezed light include quantum cryptography whereby secret keys are securely distributed to two distant parties.

Also, experimental quantum optics has enabled many fundamental theories of quantum mechanics to be tested at an unprecedented level. In particular, nonlinear processes in quantum optics have proved useful in checking the counter-intuitive predictions of the theory of quantum mechanics. For example, in [10], entangled states of light produced from squeezed states have been used to experimentally demonstrate the “spooky action at a distance” phenomenon as described by Einstein in [11]. Squeezed states of light may be used to demonstrate the EPR paradox which has been a highly controversial topic among physicists for generations, questioning the completeness of quantum theory.

## 3. Generation of Squeezed states

Nonlinear optical processes are characterized by intensity dependent effects that are quadratic or higher in the electric field vector. The polarization vector of a given medium can be written as the power series

$$P = \epsilon_0 [\chi^{(1)}E + \chi^{(2)}E^2 + \chi^{(3)}E^3 + \cdots], \tag{3}$$

where $\epsilon_0$ is the permittivity of free space, $E$ is the scalar electric field incident on the medium and $\chi^{(n)}$ are the linear and nonlinear susceptibilities of the medium. The various susceptibilities are responsible for different optical phenomena. Linear optical effects are characterized by the first order $\chi^{(1)}$ term such as the electro-optic and photo-elastic effects. The higher order susceptibilities define the area of non-linear optics. $\chi^{(2)}$ processes include parametric amplification

and second harmonic generation while $\chi^{(3)}$ processes describe third harmonic generation and the optical Kerr effect among others. For the generation of squeezed states, the $\chi^{(2)}$ processes are considered.

The generation of squeezed light was first experimentally demonstrated in 1985 [12]. It can be generated from coherent light using nonlinear optical crystals (such as magnesium oxide doped with lithium niobate) in what is known as an optical parametric amplifier/oscillator (OPA/OPO). Since then, experimental efforts have been targeted towards maximising the squeezing that can be achieved and recently, the OPO was used to successfully generate squeezed vacuum states, achieving a suppression level of about 10 dB [13]. The OPO ensures noiseless *phase-sensitive amplification* of the quadratures of light such that one of the quadratures is amplified by a certain amount and the other quadrature is de-amplified accordingly. In this way, the product of the gains in the two quadratures is unity (assuming initial minimum uncertainty).

By comparison, traditional amplifiers (such as electronic amplifiers) affect both the signal and the noise in the same way, maintaining more or less the same signal to noise ratio. Regular optical amplifiers, on the other hand, introduce additional sources of noise (referred to as vacuum states which are at the quantum noise limit) in the amplification process. These vacuum states are then amplified just like the signal such that the signal to noise ratio suffers a penalty of 3 dB [4]. This is however only the case when the amplifier acts equally on both quadratures and such amplifiers are called *phase insensitive*. To avoid this problem, we consider OPAs. In the next section, we give a brief overview of how the OPA works; see [3, 2] for more details.

### *3.1. Optical Parametric Amplification*

Certain classes of crystals show nonlinear dielectric properties, which in addition to a linear response to an electric field, propagate electromagnetic radiation whose polarization is proportional to the square of the field. With incident fields of high strength (such as lasers) and appropriate index-matching techniques [3], these second order nonlinear effects become significant. Crystals capable of showing such properties are responsible for the exchange of energy between electromagnetic fields of different frequencies, which can happen in a few different ways as follows:

1. The electromagnetic field going through a dielectric material forms temporary dipoles in the material which at high enough field strengths form a polarization wave and is re-radiated as an electromagnetic field. The re-radiated field contains numerous frequency components but for our purposes, we shall consider only second-order harmonic frequencies and optical $\chi^{(2)}$ processes. Thus, part of the energy of an optical field at frequency $f$ results in the generation of another optical field at frequency $2f$ in a process called "second harmonic generation" (SHG).
2. A fraction of a strong electromagnetic field at frequency $f_3$ simultaneously generates optical fields at frequencies $f_1$ and $f_2$, with $f_1 + f_2 = f_3$ in a process called "difference frequency generation" (DFG). In the presence of a field at frequency $f_2$, this results in what is known as a two-photon stimulated emission process and the lower frequency input field $f_2$ is amplified. This process is known as "optical parametric amplification" (OPA). Furthermore, if the nonlinear material is placed inside an optical resonator, the generated fields can build up to large values and the device becomes known as an "optical parametric oscillator" (OPO). Optical parametric oscillation occurs at some threshold intensity when the parametric gain causes simultaneous oscillations at frequencies $f_1$ and $f_2$. The output frequencies can be altered by using some phase matching properties (angle of orientation/temperature) of the nonlinear crystal.
3. A weak optical field of low frequency $f_1$ is converted to an optical field of higher frequency $f_3$ by interacting with a strong optical field $f_2$, with $f_2 = f_3 - f_1$ in a process called "frequency up-conversion".

Optical parametric amplification (Case 2) is fundamentally similar to second harmonic generation (Case 1), with the only difference being in the direction of power flow. In the special case where $f_1 = f_2$, the two processes are exactly the reverse of each other and this results in what is known as "degenerate parametric amplification". It can be shown that for parametric oscillation to occur, the pump frequency $f_3$ needs to be twice that of the signal frequency $f_1$ (or $f_2$), and that the pump phase $\phi$ relative to the signal phase must be 0 or an integer multiple of $\pi$ [2]. Here, the pump signal refers to the high intensity electromagnetic field and the input signal is the low intensity fundamental field. Moreover, a phase shift of $\pi/2$ or $(2n + 1)\pi/2$ between the two fields, where $n$ is an integer, results in the attenuation of the input signal. The degenerate parametric amplifier thus acts as a "phase sensitive amplifier". Our focus in this paper is to model this particular process which is the basis of "squeezing" effects observed in optical experiments.

## 4. Problem Description

One of the main problems associated with the generation of squeezed states is due to what is known in the physics literature as "dephasing" or "decoherence" [14]. Decoherence occurs when a system interacts with its environment in a thermodynamically irreversible way and results in the quantum nature of the system to be leaked into the environment. In a way, it determines the quantum-classical boundary and prevents the superposition of quantum states by restricting the interference of the quantum wave-functions. Decoherence has been the subject of active research in the physics community since the 1980s and efforts have been directed towards understanding the quantum-classical transition in an effort to engineer ways to prevent it by exploiting decoherence-free subspaces and dynamical decoupling procedures such as bang-bang control. In this paper however, we shall restrict our attention to quantum noises which affect both the fundamental and second-harmonic fields in an optical cavity and also directly affect the detuning variables $\Delta_a$ and $\Delta_b$ which need to be minimised or kept close to zero if any squeezing is to be observed. The detuning variables here refer to the frequency difference between the input laser beams and the respective optical fields set-up inside the optical cavity, as would be used to generate squeezed states of light. It is defined as [4]:

$$\Delta = f_c - f_L = q\frac{c}{nL} - f_L, \tag{4}$$

where $f_c$ is the resonant frequency of the cavity, $f_L$ is the laser frequency, $nL$ is the optical path length of the cavity, $c$ is the speed of light in a vacuum and $q$ is a large integer indicating that the $q^{\text{th}}$ longitudinal cavity mode is being excited. In our case, we have two laser beams with frequency $f_L$ and $2f_L$. When the cavity is in lock ($\Delta_a = \Delta_b = 0$), these laser beams excite two longitudinal modes $q_0$ and $2q_0$.

Using suitable parameter values for the optical squeezer, we first calculate the steady-state operating point (intra-cavity field magnitudes and phases) by solving a set of nonlinear coupled equations for different input phase angles. The strength of the input fields are assumed to be constant. We also explicitly determine analytical expressions for the steady-state operating points (to first order in $\chi^{(2)}$) and compare them with numerical results obtained by solving nonlinear equations. Depending on the phase angles at which the quantum state noise is squeezed, different types of squeezed states are generated. To determine which type of squeezed state we end up with, we derive the relationship that must exist between the output fields and input fields as a result of the application of input fields of varying phases. In particular, at each operating point, we determine the optical gains of the fundamental and second harmonic fields. We show that depending on the operating point, the fundamental field is amplified or de-amplified to a varying extent. More specifically, we show that the level of amplification/de-amplification (gain) follows a cyclical pattern with respect to the phase angles of the input fields. The optical gain then determines the light quadrature that is squeezed. In this way, depending on the type of squeezed states desired (amplitude or phase squeezed states), appropriate field angles can be applied using suitable control techniques [15, 16, 17].

## 5. Modelling

An optical parametric oscillator (OPO) primarily consists of a second-order nonlinear optical medium enclosed within an optical resonator. As explained in Section 3.1, materials showing second-order nonlinearities $\chi^{(2)}$ have the ability to couple a fundamental field ($f$) to a second harmonic field ($2f$). This coupling forms the basis of operation of the OPO which works by converting an input laser wave into two output waves of lower frequency through nonlinear optical interaction. Feedback in a resonator cavity results in the build-up of the waves in a process similar to that seen in an optical laser cavity and in this way, the intracavity fields become quantum correlated, resulting in the generation of squeezed states of light. For more details, the interested reader is referred to [4, 5] and [3].

### *5.1. Optical Resonator Cavity*

A schematic of an OPO driven by two optical fields $\hat{A}_{in}$ and $\hat{B}_{in}$ is shown in Figure 3. The quantities $\hat{A}_{in}$ and $\hat{B}_{in}$ are the input fields which set-up the fundamental and second-harmonic intracavity fields $\hat{a}$ and $\hat{b}$. $\kappa_{a,in}$ and $\kappa_{b,in}$ are the loss rates of the input/output mirrors for the $\hat{a}$ and $\hat{b}$ fields respectively. The parameters $\kappa_{a,l}$ and $\kappa_{b,l}$ are the internal loss rates for the corresponding two fields and $\kappa_a = \kappa_{a,in} + \kappa_{a,l}$ and $\kappa_b = \kappa_{b,in} + \kappa_{b,l}$ are the associated total resonator

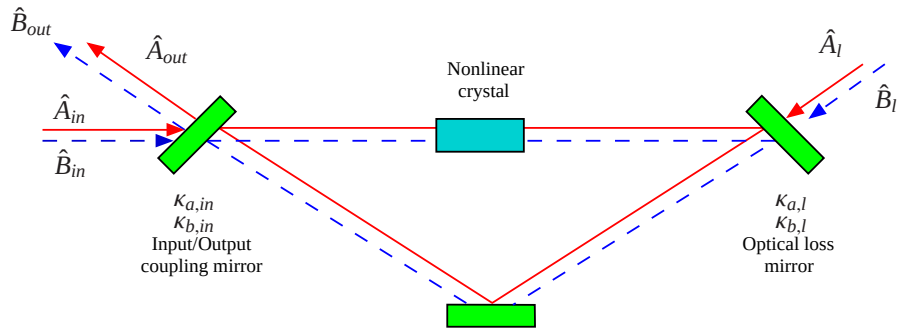


Figure 3: Schematic of an Optical Parametric Oscillator.

decay rates. Also, $\delta\hat{A}_l$ and $\delta\hat{B}_l$ represent the vacuum fields due to the internal losses. The output fields are given by $\hat{A}_{out}$ and $\hat{B}_{out}$. The quantum mechanical Hamiltonian describing the $\chi^{(2)}$ interactions is given by

$$\hat{H} = \frac{1}{2} i\chi^{(2)}(\hat{a}^{\dagger 2}\hat{b} - \hat{b}^{\dagger}\hat{a}^2), \tag{5}$$

where $a(a^{\dagger})$ and $b(b^{\dagger})$ are the annihilation (creation) operators for the fundamental and second harmonic fields respectively [4]. The first term in (5) can be interpreted as the annihilation of a single photon at the second harmonic frequency and the creation of two photons at the fundamental frequency. Similarly, the second term in (5) can be interpreted as the annihilation of two photons at the fundamental frequency and the creation of a single photon at the second harmonic frequency. Bosonic fields (such as photons) obey canonical commutation relations which govern the relationship between canonical conjugate quantities. For example, the relationship between the position $x$ and momentum $p$ of a particle is given by

$$[x, p] = i\hbar, \tag{6}$$

where $[x, p] = xp - px$ and $\hbar$ is the reduced Planck's constant $(h/2\pi)$; see, e.g., [18] for more details. This relationship implies Heisenberg uncertainty principle.

The Heisenberg equations of motion for (5) are given by [4]:

$$\dot{\hat{a}} = \chi^{(2)}\hat{a}^{\dagger}\hat{b}; \tag{7a}$$

$$\dot{\hat{b}} = -i[\hat{b}, \hat{H}] = -\frac{1}{2}\chi^{(2)}\hat{a}^2. \tag{7b}$$

Using a canonical quantisation of the equations of motion of a ring cavity (a procedure first undertaken by P. Dirac) and combining it with (7), we obtain the dynamics of the OPO for the internal cavity modes as [19]:

$$\dot{\hat{a}} = -(\kappa_a + i\Delta_a)\hat{a} + \chi^{(2)}\hat{a}^{\dagger}\hat{b} + \sqrt{2\kappa_{a,in}}\hat{A}_{in} + \sqrt{2\kappa_{a,l}}\delta\hat{A}_l; \tag{8a}$$

$$\dot{\hat{b}} = -(\kappa_b + i\Delta_b)\hat{b} - \frac{1}{2}\chi^{(2)}\hat{a}^2 + \sqrt{2\kappa_{b,in}}\hat{B}_{in} + \sqrt{2\kappa_{b,l}}\delta\hat{B}_l. \tag{8b}$$

The corresponding output fields are given by:

$$\hat{A}_{out} = \sqrt{2\kappa_{a,in}}\hat{a} - \hat{A}_{in}; \tag{9a}$$

$$\hat{B}_{out} = \sqrt{2\kappa_{b,in}}\hat{b} - \hat{B}_{in}. \tag{9b}$$

*5.2. Model Description using Quadrature Operators*

The amplitude and phase quadratures operators provide a particularly useful description of the properties of light [4]. We define them here for the optical fields $\hat{a}$ and $\hat{b}$ as:

$$X_a^+ = \hat{a} + \hat{a}^{\dagger}; \qquad X_a^- = i(\hat{a}^{\dagger} - \hat{a}); \tag{10a}$$

$$X_b^+ = \hat{b} + \hat{b}^{\dagger}; \qquad X_b^- = i(\hat{b}^{\dagger} - \hat{b}). \tag{10b}$$

The quadratures of the input and noise fields can similarly be defined as:

$$X^{+}_{Ain} = \hat{A}_{in} + \hat{A}^{\dagger}_{in}; \quad X^{-}_{Ain} = i(\hat{A}^{\dagger}_{in} - \hat{A}_{in}); \tag{11a}$$
$$X^{+}_{Bin} = \hat{B}_{in} + \hat{B}^{\dagger}_{in}; \quad X^{-}_{Bin} = i(\hat{B}^{\dagger}_{in} - \hat{B}_{in}); \tag{11b}$$
$$X^{+}_{\delta A,l} = \delta\hat{A}_{l} + \delta\hat{A}^{\dagger}_{l}; \quad X^{-}_{\delta A,l} = i(\delta\hat{A}^{\dagger}_{l} - \delta\hat{A}_{l}); \tag{11c}$$
$$X^{+}_{\delta B,l} = \delta\hat{B}_{l} + \delta\hat{B}^{\dagger}_{l}; \quad X^{-}_{\delta B,l} = i(\delta\hat{B}^{\dagger}_{l} - \delta\hat{B}_{l}). \tag{11d}$$

Then, the dynamics of the optical subsystem can be rewritten in terms of the quadratures as:

$$\dot{X}^{+}_{a} = -\kappa_a X^{+}_{a} + \Delta_a X^{-}_{a} + \frac{1}{2}\chi^{(2)}(X^{+}_{a}X^{+}_{b} + X^{-}_{a}X^{-}_{b}) + \sqrt{2\kappa_{a,in}}X^{+}_{Ain} + \sqrt{2\kappa_{a,l}}X^{+}_{\delta A,l}; \tag{12a}$$
$$\dot{X}^{-}_{a} = -\kappa_a X^{-}_{a} - \Delta_a X^{+}_{a} + \frac{1}{2}\chi^{(2)}(X^{+}_{a}X^{-}_{b} - X^{-}_{a}X^{+}_{b}) + \sqrt{2\kappa_{a,in}}X^{-}_{Ain} + \sqrt{2\kappa_{a,l}}X^{-}_{\delta A,l}; \tag{12b}$$
$$\dot{X}^{+}_{b} = -\kappa_b X^{+}_{b} + \Delta_b X^{-}_{b} - \frac{1}{4}\chi^{(2)}(X^{+2}_{a} - X^{-2}_{a}) + \sqrt{2\kappa_{b,in}}X^{+}_{Bin} + \sqrt{2\kappa_{b,l}}X^{+}_{\delta B,l}; \tag{12c}$$
$$\dot{X}^{-}_{b} = -\kappa_b X^{-}_{b} - \Delta_b X^{+}_{b} - \frac{1}{2}\chi^{(2)}X^{+}_{a}X^{-}_{a} + \sqrt{2\kappa_{b,in}}X^{-}_{Bin} + \sqrt{2\kappa_{b,l}}X^{-}_{\delta B,l}. \tag{12d}$$

The output fields are similarly expressed as

$$X^{+}_{Aout} = \sqrt{2\kappa_{a,in}}X^{+}_{a} - X^{+}_{Ain}; \tag{13a}$$
$$X^{-}_{Aout} = \sqrt{2\kappa_{a,in}}X^{-}_{a} - X^{-}_{Ain}; \tag{13b}$$
$$X^{+}_{Bout} = \sqrt{2\kappa_{b,in}}X^{+}_{b} - X^{+}_{Bin}; \tag{13c}$$
$$X^{-}_{Bout} = \sqrt{2\kappa_{b,in}}X^{-}_{b} - X^{-}_{Bin}. \tag{13d}$$

For the purpose of controller design, (12a)- (12d) are then linearised resulting in a new original linear model of the system.

### *5.3. Linearised Model of the OPO*

While nonlinear properties are essential for the generation of squeezed states of light, we only need to consider first order terms in the variations to obtain elliptical contours and Gaussian distribution functions for the states [4]. Thus, we can linearise the dynamics of the optical subsystem (12a)–(12d) without losing the important characteristic features of the optical squeezer. In this way, we model the behaviour of the system for small perturbations about a

steady state operating point of the system. The linearised dynamics of the OPO are given by:

$$\begin{aligned}
\delta\dot{X}_a^+ &= -\kappa_a\delta X_a^+ + \bar{X}_a^-\Delta_a + \frac{1}{2}\chi^{(2)}(\bar{X}_b^+\delta X_a^+ + \bar{X}_b^-\delta X_a^- + \bar{X}_a^+\delta X_b^+ + \bar{X}_a^-\delta X_b^-) \\
&\quad + \sqrt{2\kappa_{a,in}}\delta X_{Ain}^+ + \sqrt{2\kappa_{a,l}}X_{\delta A,l}^+; \qquad (14a)\\
\delta\dot{X}_a^- &= -\kappa_a\delta X_a^- - \bar{X}_a^+\Delta_a + \frac{1}{2}\chi^{(2)}(\bar{X}_b^-\delta X_a^+ - \bar{X}_b^+\delta X_a^- - \bar{X}_a^-\delta X_b^+ + \bar{X}_a^+\delta X_b^-) \\
&\quad + \sqrt{2\kappa_{a,in}}\delta X_{Ain}^- + \sqrt{2\kappa_{a,l}}X_{\delta A,l}^-; \qquad (14b)\\
\delta\dot{X}_b^+ &= -\kappa_b\delta X_b^+ + \bar{X}_b^-\Delta_b - \frac{1}{2}\chi^{(2)}(\bar{X}_a^+\delta X_a^+ - \bar{X}_a^-\delta X_a^-) \\
&\quad + \sqrt{2\kappa_{b,in}}\delta X_{Bin}^+ + \sqrt{2\kappa_{b,l}}X_{\delta B,l}^+; \qquad (14c)\\
\delta\dot{X}_b^- &= -\kappa_b\delta X_b^- - \bar{X}_b^+\Delta_b - \frac{1}{2}\chi^{(2)}(\bar{X}_a^-\delta X_a^+ + \bar{X}_a^+\delta X_a^-) \\
&\quad + \sqrt{2\kappa_{b,in}}\delta X_{Bin}^- + \sqrt{2\kappa_{b,l}}X_{\delta B,l}^-. \qquad (14d)
\end{aligned}$$

The corresponding linearised output field equations are expressed as

$$\begin{aligned}
\delta X_{Aout}^+ &= \sqrt{2\kappa_{a,in}}\delta X_a^+ - \delta X_{Ain}^+; \qquad (15a)\\
\delta X_{Aout}^- &= \sqrt{2\kappa_{a,in}}\delta X_a^- - \delta X_{Ain}^-; \qquad (15b)\\
\delta X_{Bout}^+ &= \sqrt{2\kappa_{b,in}}\delta X_b^+ - \delta X_{Bin}^+; \qquad (15c)\\
\delta X_{Bout}^- &= \sqrt{2\kappa_{b,in}}\delta X_b^- - \delta X_{Bin}^-. \qquad (15d)
\end{aligned}$$

Here, $\bar{X}_a^+, \bar{X}_a^-, \bar{X}_b^+$ and $\bar{X}_b^-$ denote the steady-state values of the respective quadratures. These are determined for the given set of input fields and phase angles by solving the nonlinear coupled equations obtained by setting the derivatives in (12a)–(12d) to zero. The linearised dynamics of the system can be used for designing linear and robust controllers.

## 6. Steady-state Analysis

At steady-state, there is a steady flow of energy between the intracavity optical fields. For an optical squeezer, the flow of energy is predominantly from the second-harmonic field to the fundamental field. Here, we determine the relationship that exists between the phase of the intracavity fields and the type of squeezed states obtained. It is not possible to have both amplitude and phase quadrature squeezing at a given operating point. We choose the phase of the input fields such that suitable stable steady-state operating points are obtained, which in turn allows quantum noise squeezing in specific quadratures.

### *6.1. Exact Steady-state solution*

The nonlinearity present in the system makes it difficult to explicitly determine expressions to describe the behaviour of the optical squeezer at steady-state. We solve for the exact stable steady-state operating point of the system numerically using conventional software such as MATLAB®. In particular, we used the MATLAB® command fsolve which uses the 'Trust-Region' technique and computes the step size using Powell procedure [20]. The algorithm is efficient and can be more robust than the Gauss-Newton method especially when starting far from a solution. The parameter values we use are chosen to reflect those of an optical squeezer in our optics laboratory and are shown in Table 1.

Using this numerical approach, it was found that for any combination of field inputs $\hat{A}_{in}$ and $\hat{B}_{in}$, we always obtain one stable steady-state solution. An analytical examination of the steady-states and the stability of nonlinear optical systems is given in [21], where the interaction of a light beam with its second-harmonic is investigated. The paper [21] focuses on non-equilibrium steady-states and considers the use of the device as a switch, when the system transitions from different steady-states. More importantly, it is shown in [21, Section 5] that provided

$$\delta = \left(\frac{C}{2}\right)^2 + \left(\frac{B-A}{3}\right)^3 \geq 0; \qquad (16)$$

Table 1: Optical Parametric Oscillator Model Parameter Values.

| Model parameter | Value | Units |
|---|---|---|
| $\kappa_a$ | $1 \times 10^5$ | rad/s |
| $\kappa_b$ | $1 \times 10^9$ | rad/s |
| $\kappa_{a,l}$ | $5 \times 10^3$ | rad/s |
| $\kappa_{b,l}$ | $5 \times 10^7$ | rad/s |
| $\kappa_{a,in}$ | $9.5 \times 10^4$ | rad/s |
| $\kappa_{b,in}$ | $9.5 \times 10^8$ | rad/s |
| $\chi^{(2)}$ | $3 \times 10^{-2}$ | – |
| $\bar{A}_{in}$ | $2 \times 10^6$ | $\sqrt{\text{rad/s}}$ |
| $\bar{B}_{in}$ | $2 \times 10^{10}$ | $\sqrt{\text{rad/s}}$ |

where

$$A = \frac{2|\bar{B}_{in}|}{\chi^{(2)}}, \quad B = \frac{2\kappa_a\kappa_b}{{\chi^{(2)}}^2}, \quad \text{and} \quad C = \frac{2\kappa_b|\bar{A}_{in}|}{{\chi^{(2)}}^2};$$

then there exists only one stable equilibrium point for the nonlinear system. Condition (16) is satisfied by the parameter values of our model in Table 1. The stability of the steady-state solution can be checked by substituting the resulting steady-state values $\bar{X}_a^+, \bar{X}_a^-, \bar{X}_b^+$ and $\bar{X}_b^-$ in (14a)– (14d) and calculating the eigenvalues of the corresponding linearised system.

### *6.2. Steady-state solution to first order in $\chi^{(2)}$*

It is also possible to obtain explicit expressions for the steady-state solution if we allow for some approximation in solving for $\hat{a}$ and $\hat{b}$ in (8a)–(8b). Since $\chi^{(2)}$ represents the small nonlinearity that couples the two optical fields, we approximate the solution to our system by considering only first order terms in $\chi^{(2)}$. It is known that the higher order terms contribute only small components to the exact solution and this justifies our assumption. Here, we derive expressions for those equilibrium operating point(s) using both polar coordinates and the field quadratures.

#### *6.2.1. Polar form solution*

The steady-state solution of the system (to first-order in $\chi^{(2)}$) is determined by equating (8a) and (8b) to zero and solving for $\hat{a}$ and $\hat{b}$:

$$-\kappa_a\hat{a} + \chi^{(2)}\hat{a}^\dagger\hat{b} + \sqrt{2\kappa_{a,in}}\hat{A}_{in} = 0; \tag{17a}$$

$$-\kappa_b\hat{b} - \frac{1}{2}\chi^{(2)}\hat{a}^2 + \sqrt{2\kappa_{b,in}}\hat{B}_{in} = 0. \tag{17b}$$

From (17b),

$$\hat{b} = -\frac{1}{\kappa_b}\left(\frac{1}{2}\chi^{(2)}\hat{a}^2 - \sqrt{2\kappa_{b,in}}\hat{B}_{in}\right). \tag{18}$$

Substituting (18) into (17a), and keeping terms linear in $\chi^{(2)}$, we have

$$-\kappa_a\hat{a} + \chi^{(2)}\hat{a}^\dagger\frac{\sqrt{2\kappa_{b,in}}}{\kappa_b}\hat{B}_{in} + \sqrt{2\kappa_{a,in}}\hat{A}_{in} = 0. \tag{19}$$

Taking the conjugate transpose of (19), we have

$$-\kappa_a\hat{a}^\dagger + \chi^{(2)}\hat{a}\frac{\sqrt{2\kappa_{b,in}}}{\kappa_b}\hat{B}_{in}^\dagger + \sqrt{2\kappa_{a,in}}\hat{A}_{in}^\dagger = 0. \tag{20}$$

From (20),

$$\hat{a}^\dagger = \chi^{(2)} \frac{\sqrt{2\kappa_{b,in}}}{\kappa_a \kappa_b} \hat{a} \hat{B}_{in}^\dagger + \frac{\sqrt{2\kappa_{a,in}}}{\kappa_a} \hat{A}_{in}^\dagger. \tag{21}$$

Substituting (21) into (19) and keeping terms linear in $\chi^{(2)}$, we can determine

$$\hat{a} = 2\chi^{(2)} \frac{\sqrt{\kappa_{a,in}\kappa_{b,in}}}{\kappa_a^2 \kappa_b} \hat{A}_{in}^\dagger \hat{B}_{in} + \frac{\sqrt{2\kappa_{a,in}}}{\kappa_a} \hat{A}_{in}^\dagger. \tag{22}$$

Finally substituting (22) into (18), we have

$$\hat{b} = \frac{\sqrt{2\kappa_{b,in}}}{\kappa_b} \hat{B}_{in} - \chi^{(2)} \frac{\kappa_{a,in}}{\kappa_a^2 \kappa_b} \hat{A}_{in}^2. \tag{23}$$

If we denote the steady-state values of the fields $\hat{a}$ and $\hat{b}$ by $\bar{a}$ and $\bar{b}$ respectively, we can rewrite the steady-state values of the fundamental and the second-harmonic fields as:

$$\bar{a} = e^{i\bar{\theta}_{a,in}} \left[ \frac{\sqrt{2\kappa_{a,in}}}{\kappa_a} |\bar{A}_{in}| + 2\chi^{(2)} \frac{\sqrt{\kappa_{a,in}\kappa_{b,in}}}{\kappa_a^2 \kappa_b} |\bar{A}_{in}||\bar{B}_{in}| e^{i(\bar{\theta}_{b,in} - 2\bar{\theta}_{a,in})} \right]; \tag{24a}$$

$$\bar{b} = e^{i\bar{\theta}_{b,in}} \left[ \frac{\sqrt{2\kappa_{b,in}}}{\kappa_b} |\bar{B}_{in}| - \chi^{(2)} \frac{\kappa_{a,in}}{\kappa_a^2 \kappa_b} |\bar{A}_{in}|^2 e^{-i(\bar{\theta}_{b,in} - 2\bar{\theta}_{a,in})} \right]; \tag{24b}$$

where the steady state values of the input fields are expressed in polar coordinates as $\bar{A}_{in} = |\bar{A}_{in}| e^{i\bar{\theta}_{a,in}}$ and $\bar{B}_{in} = |\bar{B}_{in}| e^{i\bar{\theta}_{b,in}}$. Also, we write $\bar{a} = |\bar{a}| e^{i\bar{\theta}_a}$ and $\bar{b} = |\bar{b}| e^{i\bar{\theta}_b}$.

*6.2.2. Solution in terms of the field quadratures*

The steady-state solution of the optical system (to first-order in $\chi^{(2)}$) can also be expressed by expanding the field quadratures in terms of their coherent amplitude and quantum noise operators, so that a quadrature $X_i^\pm = \bar{X}_i^\pm + \delta X_i^\pm$, $i = a, b$ where $\bar{X}_i^\pm$ and $\delta X_i^\pm$ represent the expectation value and small variations of the field quadratures respectively. The expectation value of the field quadratures (to first order in $\chi^{(2)}$) are correspondingly given by:

$$\bar{X}_a^+ = \frac{\sqrt{2\kappa_{a,in}}}{\kappa_a} (\bar{A}_{in} + \bar{A}_{in}^\dagger) + 2\chi^{(2)} \frac{\sqrt{\kappa_{a,in}\kappa_{b,in}}}{\kappa_a^2 \kappa_b} (\bar{A}_{in}^\dagger \bar{B}_{in} + \bar{A}_{in} \bar{B}_{in}^\dagger); \tag{25a}$$

$$\bar{X}_a^- = i \left[ \frac{\sqrt{2\kappa_{a,in}}}{\kappa_a} (\bar{A}_{in}^\dagger - \bar{A}_{in}) + 2\chi^{(2)} \frac{\sqrt{\kappa_{a,in}\kappa_{b,in}}}{\kappa_a^2 \kappa_b} (\bar{A}_{in} \bar{B}_{in}^\dagger - \bar{A}_{in}^\dagger \bar{B}_{in}) \right]; \tag{25b}$$

$$\bar{X}_b^+ = \frac{\sqrt{2\kappa_{b,in}}}{\kappa_b} (\bar{B}_{in} + \bar{B}_{in}^\dagger) - \chi^{(2)} \frac{\kappa_{a,in}}{\kappa_a^2 \kappa_b} (\bar{A}_{in}^2 + \bar{A}_{in}^{\dagger 2}); \tag{25c}$$

$$\bar{X}_b^- = i \left[ \frac{\sqrt{2\kappa_{b,in}}}{\kappa_b} (\bar{B}_{in}^\dagger - \bar{B}_{in}) - \chi^{(2)} \frac{\kappa_{a,in}}{\kappa_a^2 \kappa_b} (\bar{A}_{in}^{\dagger 2} - \bar{A}_{in}^2) \right]. \tag{25d}$$

## 7. Steady-state Behaviour

The effect of various parameters (in particular the phase angles of the input fields) on the system are analysed at steady-state, using both the exact numerical method and the approximate equations described in Section 6.2. Here, we represent the results graphically using the parameters in Table 1, except for the ones specifically identified. First, we investigate the effect of changing the phase $\bar{\theta}_{a,in}$ of the input field $\hat{A}_{in}$ on the intracavity field phase angle $\bar{\theta}_a$. The phase of the input field is varied from 0 to $2\pi$.

Figure 4(a) shows the phase of the fundamental intracavity field following that of the fundamental input field very closely for $\bar{\theta}_{b,in} = 0$. Moreover, the solution obtained using only linear terms in $\chi^{(2)}$ and the nonlinear one can be seen to agree very closely with each other, implying that it is reasonable to work with only the linear terms in most cases.

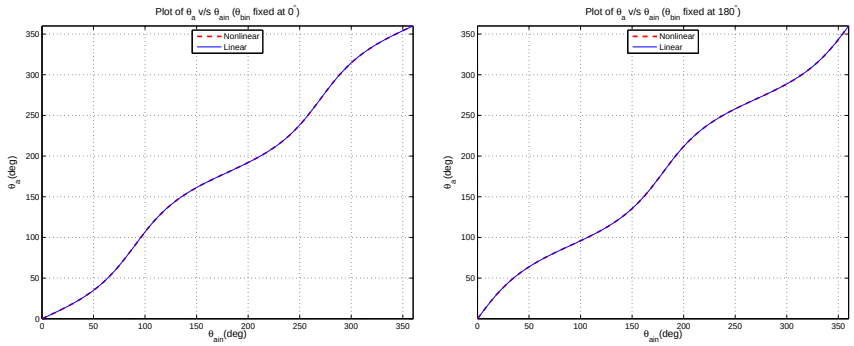


(a) $\bar{\theta}_{b,in} = 0$ (b) $\bar{\theta}_{b,in} = \pi$

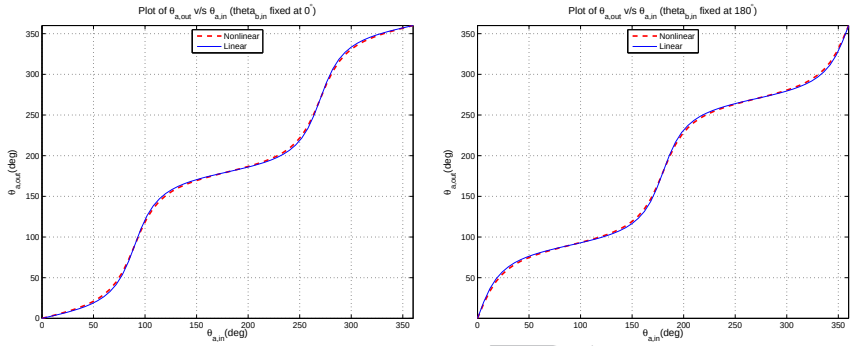


(c) $\bar{\theta}_{b,in} = 0$ (d) $\bar{\theta}_{b,in} = \pi$

Figure 4: Variation of $\bar{\theta}_a$ and $\bar{\theta}_{a,out}$ with respect to $\bar{\theta}_{a,in}$.

The procedure is repeated at a different phase angle $\bar{\theta}_{b,in} = \pi$ for the harmonic input field $\hat{B}_{in}$ and a similar relationship is seen; see Figure 4(b). In Figure 4(c) and 4(d), we show the variation of the phase $\bar{\theta}_{a,out}$ of the fundamental output field $\hat{A}_{out}$, with the phase of the input field $\bar{\theta}_{a,in}$. We choose the same combination of phase angles $\bar{\theta}_{b,in}$ as above. It can be seen that the following approximations hold true at steady-state:

$$\bar{\theta}_{a,out} \simeq \bar{\theta}_a \simeq \bar{\theta}_{a,in}. \tag{26}$$

The variation of the phase of the intracavity field $\hat{b}$ and the output field $\hat{B}_{out}$ with the phase of the input field $\hat{A}_{in}$ is also determined. We found that varying $\bar{\theta}_{a,in}$ does not have any noticeable effect on the second harmonic output fields. This result is as expected given the large difference in the field strengths of the input fields $\hat{A}_{in}$ and $\hat{B}_{in}$ and the predominant direction of energy flow in the OPO at steady-state.

Next, we consider the variation of the phase angle $\bar{\theta}_{a,out}$ of the output field $\hat{A}_{out}$, with respect to the phase $\bar{\theta}_{b,in}$ of the second harmonic input field $\hat{B}_{in}$. Figure 5 shows that the input field $\hat{B}_{in}$ has considerable effect on the output field $\hat{A}_{out}$. This is again as expected given the strength of the second harmonic field.

We repeat the above procedure for the second harmonic field. It is found that the phase $\bar{\theta}_b$ of the intracavity field $\hat{b}$ varies linearly with respect to the phase $\theta_{b,in}$ of the input field $\hat{B}_{in}$, as shown in Figure 6. Moreover, the phase of the output field $\bar{\theta}_{b,out}$ follows $\bar{\theta}_b$ very closely. We thus obtain the approximation:

$$\bar{\theta}_{b,out} \simeq \bar{\theta}_{b,in} \simeq \bar{\theta}_b. \tag{27}$$

Figure 7(a) and Figure 7(b) show the variation of the magnitude of the intracavity field $\hat{a}$ with respect to $\bar{\theta}_{a,in}$. We consider two cases when $\bar{\theta}_{b,in} = 0$ and $\pi$. It is clear that there is a large change in the strength of the intracavity field $\hat{a}$ which is cyclical in nature as the phase angle $\bar{\theta}_{a,in}$ is varied. Similarly, Figure 7(c) and Figure 7(d) show the variation of the magnitude of intracavity field $\hat{a}$ with respect to $\bar{\theta}_{b,in}$. Here, we consider two cases when $\bar{\theta}_{a,in} = 0$ and $\pi$. The

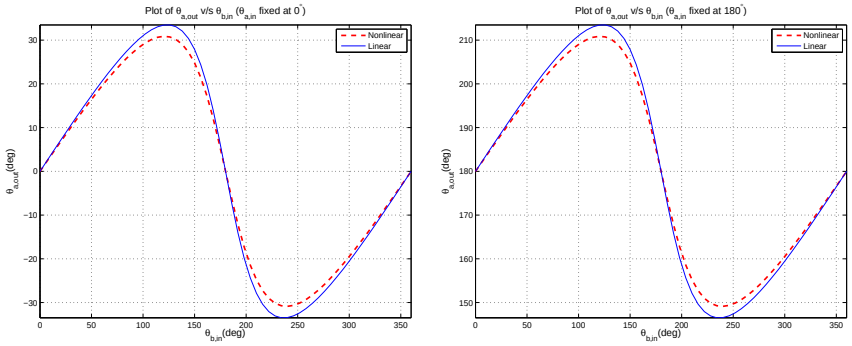


(a) $\bar{\theta}_{a,in} = 0$ (b) $\bar{\theta}_{a,in} = \pi$

Figure 5: Variation of $\bar{\theta}_{a,out}$ with respect to $\bar{\theta}_{b,in}$.

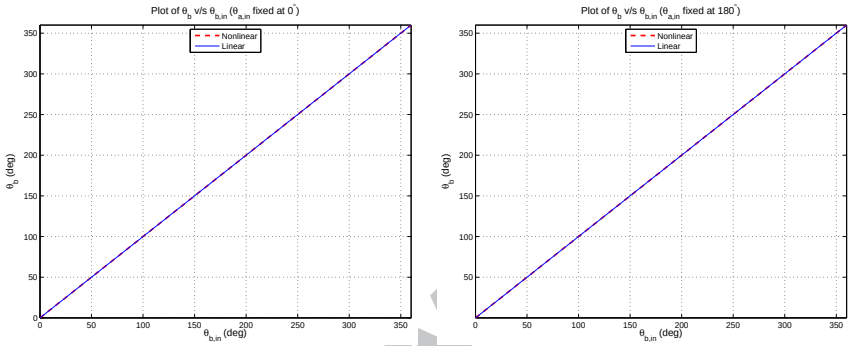


(a) $\bar{\theta}_{a,in} = 0$ (b) $\bar{\theta}_{a,in} = \pi$

Figure 6: Variation of $\bar{\theta}_b$ with respect to $\bar{\theta}_{b,in}$.

variation of field $\hat{a}$ goes through only one cycle as we vary $\bar{\theta}_{b,in}$ from 0 to $2\pi$ in this case. This is as expected since the frequency of input field $\hat{B}_{in}$ is twice that of the input field $\hat{A}_{in}$. Thus, the system behaves as a *phase sensitive* amplifier. Also, it should be noted that the approximate and nonlinear solutions show similar behaviour but quite a significant difference in numerical values is obtained in this case.

Next, we analyse the optical parametric gain of the fundamental and harmonic fields, i.e., the ratio of $|\hat{A}_{out}|^2/|\hat{A}_{in}|^2$ and $|\hat{B}_{out}|^2/|\hat{B}_{in}|^2$. Figures 8(a) and 8(b) show the variation of $|\hat{A}_{out}|^2/|\hat{A}_{in}|^2$ and $|\hat{B}_{out}|^2/|\hat{B}_{in}|^2$ with respect to the phase angle $\bar{\theta}_{a,in}$ of the fundamental input field $\hat{A}_{in}$. Similarly, Figures 8(c) and 8(d) show the variation of the gain $|\hat{A}_{out}|^2/|\hat{A}_{in}|^2$ and $|\hat{B}_{out}|^2/|\hat{B}_{in}|^2$ with respect to the phase angle $\bar{\theta}_{b,in}$ of the harmonic input field $\hat{B}_{in}$. The gain $|\hat{B}_{out}|^2/|\hat{B}_{in}|^2$ of the harmonic field is negligible and barely changes with the phase angles of the input fields. On the other hand, the optical field $\hat{A}_{out}$ is clearly affected in all of the figures. Again, the variation of the gain $|\hat{A}_{out}|^2/|\hat{A}_{in}|^2$ is seen to go through 2 cycles when $\bar{\theta}_{a,in}$ is varied, compared to only one cycle with variation in $\bar{\theta}_{b,in}$. Figure 8 also shows that the gain $|\hat{A}_{out}|^2/|\hat{A}_{in}|^2$ can be controlled by fixing either $\bar{\theta}_{a,in}$ or $\bar{\theta}_{b,in}$ and varying the other field angle.

The effect of $\chi^{(2)}$ on the gain is investigated next. In Figure 9, we vary the phase $\bar{\theta}_{a,in}$ of the input field $\hat{A}_{in}$ and determine its effect on the gain $|\hat{A}_{out}|^2/|\hat{A}_{in}|^2$ of the fundamental field. We repeat the process for different parameter values of $\chi^{(2)}$. We find that the parameter $\chi^{(2)}$ significantly affects the gain of the optical field $|\hat{A}_{out}|^2/|\hat{A}_{in}|^2$. Increasing $\chi^{(2)}$ increases the coupling between the fields $\hat{A}$ and $\hat{B}$ which in turn increases the steady-state energy flow from intracavity field $\hat{b}$ to $\hat{a}$. However, this effect is reversed beyond a certain value of $\chi^{(2)}$ as seen for the cases when when $\chi^{(2)} = 0.7$ and 1.5. To show this effect more clearly, we select a pair of values for $\bar{\theta}_{a,in}$ and $\bar{\theta}_{b,in}$ and investigate the effect of varying $\chi^{(2)}$ on the gain $|\hat{A}_{out}|^2/|\hat{A}_{in}|^2$ of the fundamental field. Figure 10 shows that the optimal gain

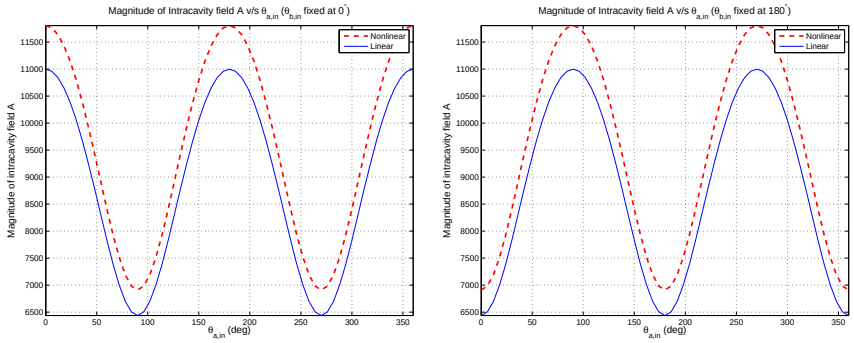


(a) Field $|\hat{a}|$ at $\bar{\theta}_{b,in} = 0$ (b) Field $|\hat{a}|$ at $\bar{\theta}_{b,in} = \pi$

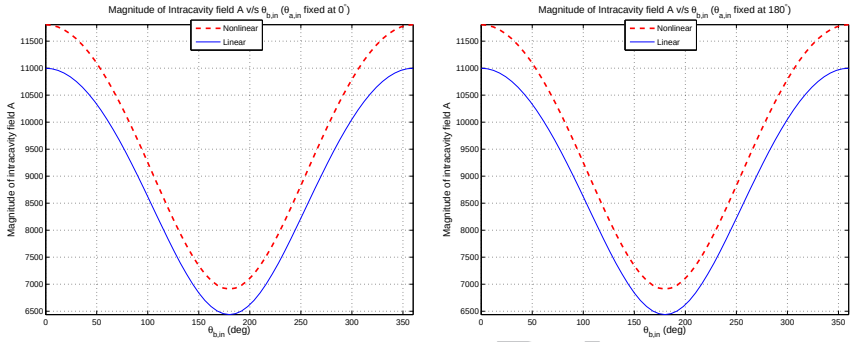


(c) Field $|\hat{a}|$ at $\bar{\theta}_{a,in} = 0$ (d) Field $|\hat{a}|$ at $\bar{\theta}_{a,in} = \pi$

Figure 7: Variation of the magnitude of the intracavity field $\hat{a}$ with respect to $\bar{\theta}_{a,in}$ and $\bar{\theta}_{b,in}$.

$|\hat{A}_{out}|^2/|\hat{A}_{in}|^2$ can be achieved at a $\chi^{(2)} \approx 0.115$. However, nonlinear materials with such large values of $\chi^{(2)}$ are not practically realisable. Moreover, it is well known that $\chi^{(2)}$ is a function of numerous factors, including temperature, electromagnetic field strength and angle of orientation [3], making it extremely difficult to operate at any optimally chosen value.

It must be emphasized that the simulation results obtained for the linear and nonlinear models agree with experimental results that have been performed in the physics community [8, 13]. However, the emphasis in the physics community, has been on achieving the maximum level of squeezing and naturally optimality is assumed about the operating point, with the phase of the input fields being tightly regulated. We are in the context of this paper more interested in showing the effect of widely varying the phase angles and this aspect of the work has not been considered before in experimental work, in the literature. Also, as the original aim of developing the math model for the dynamical system is to design controllers to regulate the phase angle, this aspect of the model is clearly demonstrated here to justify the need for designing controllers.

## 8. Summary of Results

The analysis performed in the previous sections is summarised here in an attempt to formulate a suitable mathematical condition that results in the generation of a specific type of squeezed states of light. We consider the variation of the steady-state gain of the OPO under some specific conditions which are satisfied in the set-up shown in Figure 3. If $\kappa_a << \kappa_b$, and the harmonic field $\hat{B}_{in}$ is much more intense than the fundamental field $\hat{A}_{in}$, then energy will be predominantly transferred from field $\hat{b}$ to field $\hat{a}$. The steady-state optical gain of the fundamental field $|\hat{A}_{out}|^2/|\hat{A}_{in}|^2$, is then of much greater magnitude than the corresponding gain with respect to the field $\hat{b}$. In fact, we have shown that field $\hat{b}$ is virtually undepleted by its interaction with field $\hat{a}$ when the above conditions are met; see Figure 8. Here, we determine the variation of the gain $|\hat{A}_{out}|^2/|\hat{A}_{in}|^2$ with respect to the quantities $\bar{\theta}_{a,in}$ and $\bar{\theta}_{b,in}$. This is equivalent to

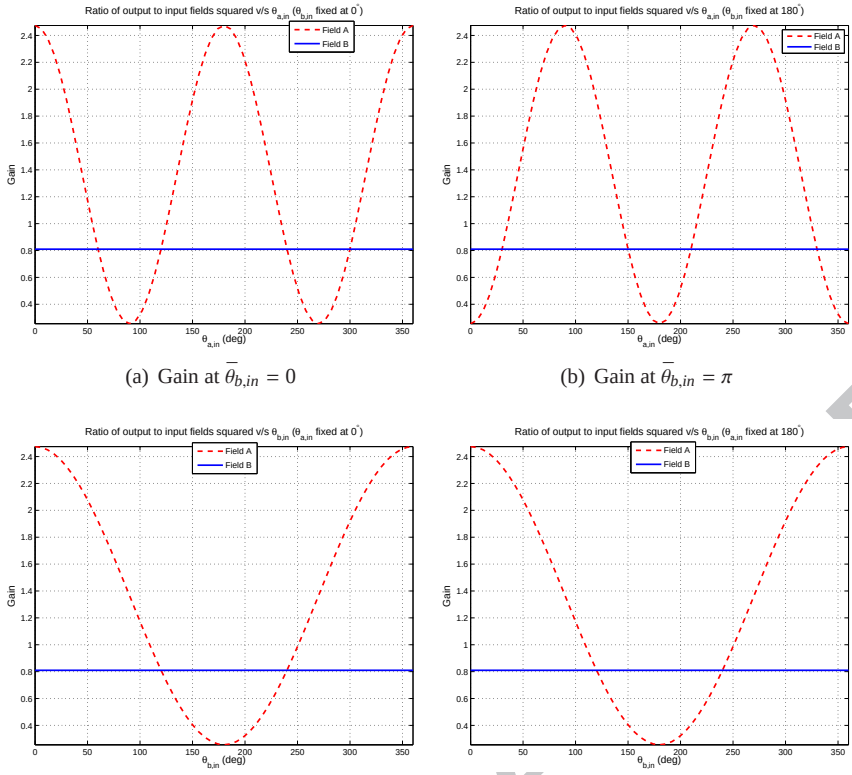


(a) Gain at $\bar{\theta}_{b,in} = 0$ (b) Gain at $\bar{\theta}_{b,in} = \pi$

(c) Gain at $\bar{\theta}_{a,in} = 0$ (d) Gain at $\bar{\theta}_{a,in} = \pi$

Figure 8: Variation of gain $|\hat{A}_{out}|^2/|\hat{A}_{in}|^2$ and $|\hat{B}_{out}|^2/|\hat{B}_{in}|^2$.

combining numerous plots of the type shown in Figure 8 for the fundamental field for different phase angles and the result is shown in Figure 11. The variation of the gain $|\hat{A}_{out}|^2/|\hat{A}_{in}|^2$ with respect to the phase angles of the input fields is used in the determination of the operating point we would choose to obtain maximum squeezing. In particular, depending on the quadrature we would like to squeeze, we choose appropriate operating point(s) corresponding to a given pair of input field angles $\bar{\theta}_{a,in}$ and $\bar{\theta}_{b,in}$ such that we have the appropriate level of steady-state gain $|\hat{A}_{out}|^2/|\hat{A}_{in}|^2$.

Figure 12 illustrates the way in which we determine the type and extent of the quadrature squeezing achieved. It shows the effect of varying the steady-state gain $|\hat{A}_{out}|^2/|\hat{A}_{in}|^2$ of a coherent state of light (minimum uncertainty state) denoted $\hat{A}_{out}$. The symmetric circular region represents the uncertainty associated with a given coherent state due to quantum noise. This noise is equally divided between the two quadratures. The diagram shows how amplifying one quadrature by a given amount and de-amplifying the other quadrature by the same amount, a process which does not violate the Heisenberg uncertainty relation, results in a quadrature with an uncertainty level below the SQL. The gain here is, of course, introduced by a phase-sensitive amplifier or parametric amplifier, as provided by an OPO. We can thus change the noise distribution about the state from being circular and symmetric about the quadratures to elliptical and asymmetric. In particular, the noise variance along a given quadrature increases while that along the other (orthogonal) quadrature decreases proportionately such that the Heisenberg uncertainty principle is not violated

$$\langle \delta X_{Aout}{}^{+2} \rangle \langle \delta X_{Aout}{}^{-2} \rangle \geq 1. \tag{28}$$

Figure 12 also shows that increasing the steady-state gain results in phase squeezing while decreasing the gain gives rise to amplitude squeezing. If we are interested in maximising the level of amplitude squeezing, we would then ideally operate in a region where the optical steady-state gain is at its minimum. Using Figure 8 and Figure 11, we can determine the relationship between $\bar{\theta}_{a,in}$ and $\bar{\theta}_{b,in}$ when the optical gain is at its minimum. To achieve optimal

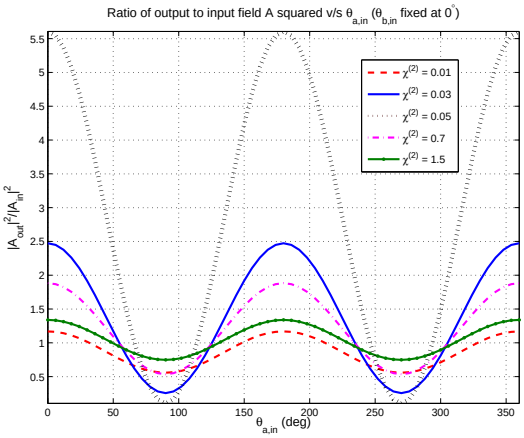


Figure 9: Variation of the gain $|\hat{A}_{out}|^2/|\hat{A}_{in}|^2$ of the fundamental output field with respect to $\theta_{a,in}$ for different $\chi^{(2)}$.

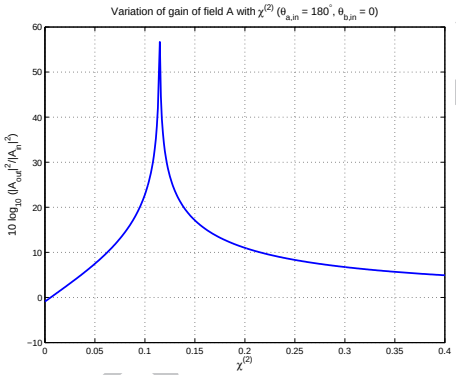


Figure 10: Variation of the parametric gain $|\hat{A}_{out}|^2/|\hat{A}_{in}|^2$ of the fundamental field (in dB) with respect to $\chi^{(2)}$.

amplitude squeezing, we would then choose the operating point so that

$$\bar{\theta}_{b,in} - 2\bar{\theta}_{a,in} = 2n\pi; \quad \text{where } n \in \mathbb{Z}; \tag{29}$$

a relationship that is well known in the experimental physics community [4]. Furthermore, the relationship between $\bar{\theta}_{a,in}$ and $\bar{\theta}_a$ and between $\bar{\theta}_{b,in}$ and $\bar{\theta}_b$ as determined from (26)–(27) show that an equivalent condition to (29) for maximum amplitude squeezing of the fundamental field $\hat{a}$ would be

$$\bar{\theta}_b - 2\bar{\theta}_a = 2n\pi. \tag{30}$$

A similar relationship can be easily derived for phase squeezing, with maximum phase squeezing of the fundamental field $\hat{a}$ occurring when

$$\bar{\theta}_b - 2\bar{\theta}_a = (2n+1)\pi. \tag{31}$$

## 9. Conclusions

In this paper, an optical squeezer has been successfully modeled and analyzed. In particular, the nonlinear optical processes by which squeezed states of light, having quadratures possessing less noise than the QNL, has been studied in detail. It is well known that depending on the applications in experimental physics, different squeezed states are

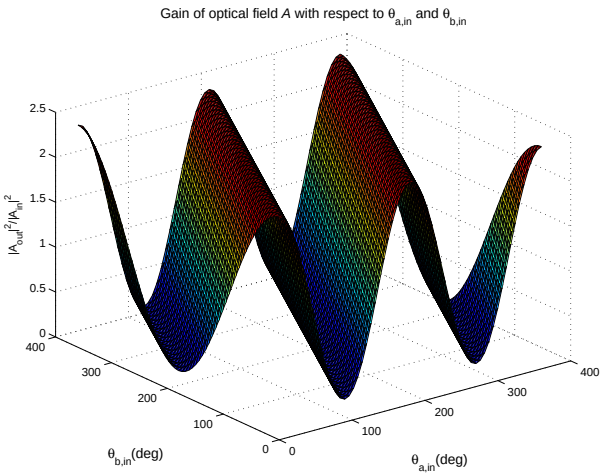


Figure 11: Variation of the gain $|\hat{A}_{out}|^2/|\hat{A}_{in}|^2$ with $\bar{\theta}_{a,in}$ and $\bar{\theta}_{b,in}$.

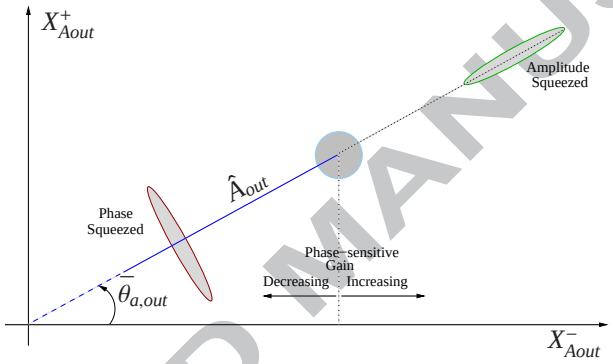


Figure 12: Representation of phase sensitive squeezing.

desired. Here, the steady-state conditions necessary for the generation of amplitude and phase squeezed states of light were determined and visually depicted. There are clearly numerous suitable operating points that can result in the generation of a specific type of squeezed state of light. It is hoped that the results obtained will help in setting and closely regulating the conditions necessary through appropriate control methodologies.

**Acknowledgements**

The author wishes to thank Prof. I. R. Petersen and Prof. E. H. Huntington for numerous discussions during the development of this work.

**References**

**References**

[1] E. Merzbacher, Quantum Mechanics, John Wiley & Sons Ltd., third edition, 1998.
[2] A. Yariv, Quantum Electronics, John Wiley & Sons Ltd., 1989.
[3] R. W. Boyd, Nonlinear Optics, Academic Press, Boston, 2008.
[4] H. A. Bachor, T. C. Ralph, A Guide to Experiments in Quantum Optics, John Wiley, 2004.
[5] C. W. Gardiner, P. Zoller, Quantum Noise, Springer, Berlin, 2000.

[6] W. Pauli, General Principles of Quantum Mechanics, Springer, 1980.
[7] C. M. Caves, Quantum-mechanical noise in an interferometer, Phys. Rev. D 23 (1981) 1693–1708.
[8] H. Vahlbruch, S. Chelkowski, B. Hage, A. Franzen, K. Danzmann, R. Schnabel, Coherent control of vacuum squeezing in the gravitational-wave detection band, Phys. Rev. Lett. 97 (2006) 011101.
[9] W. P. Bowen, N. Treps, B. C. Buchler, R. Schnabel, T. C. Ralph, H. Bachor, T. Symul, P. K. Lam, Experimental investigation of continuous-variable quantum teleportation, Phys. Rev. A 67 (2003) 032302.
[10] A. Aspect, P. Grangier, G. Roger, Experimental Realization of Einstein-Podolsky-Rosen-Bohm Gedankenexperiment: A New Violation of Bell's Inequalities, Phys. Rev. Lett. 49 (1982) 91–94.
[11] A. Einstein, B. Podolsky, N. Rosen, Can quantum-mechanical description of physical reality be considered complete?, Physical Review 47 (1935) 777–780.
[12] R. E. Slusher, L. W. Hollberg, B. Yurke, J. C. Mertz, J. F. Valley, Observation of Squeezed States Generated by Four-Wave Mixing in an Optical Cavity, Phys. Rev. Lett. 55 (1985) 2409–2412.
[13] H. Vahlbruch, M. Mehmet, S. Chelkowski, B. Hage, A. Franzen, N. Lastzka, S. Gobler, K. Danzmann, R. Schnabel, Observation of squeezed light with 10-db quantum-noise reduction, Phys. Rev. Letters 100 (2008).
[14] A. E. Siegman, Lasers, University Science Books, 1986.
[15] S. Z. Sayed Hassen, I. R. Petersen, E. H. Huntington, M. Heurs, M. R. James, LQG control of an optical squeezer, in: Proc. American Control Conf., Baltimore, MD, USA, pp. 2730–2735.
[16] S. Z. Sayed Hassen, I. R. Petersen, Optimal amplitude quadrature control of an optical squeezer using an integral LQG approach, in: IEEE Multi-Conference on Systems and Control, Yokohama, Japan, pp. 286–291.
[17] S. Z. Sayed Hassen, I. R. Petersen, E. H. Huntington, Optimal Squeezing using Multivariable Integral LQG Control, in: Proc. of the 18th IFAC World Congress, Milano, Italy, pp. 7553–7558.
[18] M. Srednicki, Quantum Field Theory, Cambridge University Press, 2007.
[19] M. J. Collett, C. W. Gardiner, Squeezing of intracavity and traveling-wave light fields produced in parametric amplification, Phys. Rev. A 30 (1984) 1386–1391.
[20] M. J. D. Powell, A Fortran Subroutine for Solving Systems of Nonlinear Algebraic Equations, Numerical Methods for Nonlinear Algebraic Equations, Gordon and Breach, London, UK, 1970.
[21] P. D. Drummond, K. J. McNeil, D. F. Walls, Non-equilibrium transitions in sub/second harmonic generation, Journal of Modern Optics 27 (1980) 321–335.